the positive $\Delta \log K$ value may be attributed to the shift from tetrahedral to octahedral coordination and concomitant water binding. The $\Delta \log K$ values for Zn(II) with phenanthroline and bipyridine are of the order expected statistically. This would indicate that both the binary and ternary complexes are essentially octahedral in these cases.

The present study shows that the coordination number, the geometry of the metal ion, and the nature of the ligands play an important role in determining the stabilities and structures of the mixed-ligand complexes. These factors may be a few of the many reasons that cause certain metal ions to catalyze and others to inhibit enzymatic reactions.

Acknowledgment. The authors gratefully acknowledge support of this research under Grant AM 21669 from the National Institutes of Health.

Registry No. Histamine, 51-45-6; 1,10-phenanthroline, 66-71-7; 2,2′-bipyridyl, 366-18-7; *O*-phospho-DL-serine, 17885-08-4; Cu, 7440-50-8; Ni, 7440-02-0; Co, 7440-48-4; Zn, 7440-66-6.

References and Notes

(1) *Metab. Pathways, 3rd Ed.*, **3**, 238 (1969).
(2) (a) F. C. Neuhaus and W. L. Byrne, *J. Biol. Chem.*, **234**, 113 (1959); (b) M. Schramm, *ibid.*, **233**, 1169 (1958).
(3) (a) A. S. Mildvan and M. Cohn, *J. Biol. Chem.*, **241**, 1178 (1966); (b) A. S. Mildvan, *Enzymes, 3rd Ed.*, **2**, 445 (1970); (c) A. S. Mildvan and M. Cohn, *Adv. Enzymol. Relat. Areas Mol. Biol.*, **33**, 1 (1970).
(4) M. S. Mohan and E. H. Abbott, *Inorg. Chem.*, **17**, 2203 (1978).
(5) H. A. Flashka, "EDTA Titrations", 2nd ed., Pergamon Press, Oxford, 1964.
(6) I. G. Sayce, *Talanta*, **15**, 1397 (1968).
(7) R. Griesser and H. Sigel, *Inorg. Chem.*, **10**, 2229 (1971).
(8) H. Irving and D. L. Mellor, *J. Chem. Soc.*, 5222 (1962).
(9) R. M. Smith and A. E. Martell, "Critical Stability Constants", Vol. 2, Plenum Press, New York, 1975.
(10) R. B. Martin and R. Prados, *J. Inorg. Nucl. Chem.*, **36**, 1665 (1974).
(11) A. L. Beauchamp, J. Israeli, and H. Saulnier, *Can. J. Chem.*, **47**, 1269 (1969).
(12) J. Israeli and H. Saulnier, *Inorg. Chim. Acta*, **2**, 482 (1968).
(13) J. Israeli and M. Cecchetti, *J. Inorg. Nucl. Chem.*, **30**, 2079 (1968).
(14) J. Israeli and J. R. Cayouette, *Can. J. Chem.*, **49**, 199 (1971).
(15) F. A. Walker, H. Sigel, and D. B. McCormick, *Inorg. Chem.*, **11**, 2756 (1972).
(16) H. Sigel, *Angew. Chem., Int. Ed. Engl.*, **14**, 394 (1975).
(17) H. Irving and R. J. P. Williams, *J. Chem. Soc.*, 3192 (1953).
(18) (a) D. D. Perrin, I. G. Sayce, and V. J. Sharma, *J. Chem. Soc. A*, 1755 (1967); (b) D. D. Perrin and V. S. Sharma, *ibid.*, 446 (1968); (c) D. D. Perrin and V. S. Sharma, *ibid.*, 2060 (1969).
(19) H. C. Freeman, *Adv. Protein Chem.*, **22**, 257 (1967).
(20) (a) R. Kretzinger, F. A. Cotton, and E. F. Bryan, *Acta Crystallogr.*, **16**, 651 (1953); (b) M. M. Harding and S. J. Cole, *ibid.*, **16**, 643 (1963); (c) D. D. Perrin and V. J. Sharma, *J. Chem. Soc. A*, 742 (1967).
(21) G. Anderegg, *Helv. Chim. Acta*, **44**, 1673 (1961).

Contribution from the Department of Chemistry,
The University of North Carolina, Chapel Hill, North Carolina 27514

Anisotropic Mixed-Valence Systems. Dimers of the Delocalized Clusters $[Ru_3O(CH_3CO_2)_6(L)_3]^{n+}$

JOHN A. BAUMANN, DENNIS J. SALMON, STEPHEN T. WILSON, and THOMAS J. MEYER*

Received December 15, 1978

A series of ligand-bridged cluster dimers of the type $[(py)_2Ru_3O(CH_3CO_2)_6(L)Ru_3O(CH_3CO_2)_6(py)_2]^{2+}$ (L = pyrazine (pyr), 4,4′-bipyridine (4,4′-bpy), *trans*-1,2-bis(4-pyridyl)ethylene (BPE), 1,2-bis(4-pyridyl)ethane (BPA); pyridine (py)) has been prepared. As shown by cyclic voltammetry, the extensive reversible redox chemistry of the individual clusters, e.g., $[Ru_3O(CH_3CO_2)_6(py)_2(pyr)]^{3+/2+/+/0/-/2-}$, appears in the dimers but is even more complex. In the individual clusters, electrons are gained or lost from a series of delocalized, intracluster levels and it is concluded that in the dimers the cluster units can be treated as single "super" redox sites with regard to electronic interactions through the bridging ligands. The extent of intercluster interaction depends both on the bridging ligand and on the electron content of the clusters. In the "mixed-valence" dimers $[(py)_2Ru_3O(CH_3CO_2)_6(pyr)Ru_3O(CH_3CO_2)_6(py)_2]^{m+}$ (m = 1, 3), there appear to be discrete (Ru_3O^+–$Ru^0{}_3O$ or $Ru^{2+}{}_3O$–Ru^+) cluster sites and difference spectra in the near-infrared region provide evidence for low-energy cluster–cluster charge transfer (CCCT) or intervalence transfer (CCIT) absorption bands. Intercluster electronic coupling appears to increase with electron content and in the 1– mixed-valence dimer may be sufficient that the dimer is delocalized.

Introduction

In the study of mixed-valence compounds, the systems chosen for study have largely been symmetrical dimers with a ligand bridging two metal sites, e.g., $(C_5H_5)Fe(C_5H_4$–$C_5H_4)Fe(C_5H_5)$, $[(NH_3)_5Ru(pyr)Ru(NH_3)_5]^{4+}$, and $[(bpy)_2ClRuORuCl(bpy)_2]^{2+}$.[1] Oxidation of the dimers leads to mixed-valence ions for which an adequate description of oxidation state can be difficult to obtain. In one limiting case the excess electron is trapped on one of the metal sites because of differences which exist in the equilibrium inner- and outer-coordination spheres of the metal in the two different oxidation states. In a second, electronic coupling between the sites is sufficiently strong to overcome the vibrational trapping energy and create a new chemical system in which the inner- and outer-coordination spheres at the two metal sites are equivalent. Electronic coupling occurs by orbital overlap which can be promoted by mixing with appropriate orbitals of the bridging ligand. Closely related chemical examples are known where the two different limiting cases have been found.[1-7]

The description of oxidation state in mixed-valence systems and the transition between different limiting forms pose problems of description similar to those which occur in other areas of chemistry including valence tautomerisms in organic chemistry and Jahn–Teller distortions. Mixed-valence systems are important candidates for the study of such problems because systematic variations can be made in the redox sites, in nonbridging ligands, and in the connecting chemical link between the redox sites.

We have extended[8,9] the earlier work of Spencer and Wilkinson[10,11] on the oxo-bridged, triangular clusters $Ru_3O(CH_3CO_2)_6L_3$ (Figure 1). Electrochemical and chemical isolation studies have shown that the clusters undergo a series of reversible one-electron transfers to give the electron-transfer related clusters $Ru_3O(CH_3CO_2)_6L_3{}^{3+/2+/+/0/-}$. The results of spectral studies on the 2+, 1+, and 0 clusters suggest that the multiple electron transfers involve the gain (or loss) of electrons from a series of levels which are largely delocalized Ru–Ru or Ru–O–Ru in character.

We have developed a synthetic procedure for linking cluster units using bridging ligands like pyrazine as in the dimer $[(py)_2Ru_3O(CH_3CO_2)_6(pyr)Ru_3O(CH_3CO_2)_6(py)_2]$ (py is pyridine; pyr is pyrazine). The resulting dimers (of trimers!) are of interest to us because: (1) a redox and metal–metal interaction anisotropy exists in them since there are separate

0020-1669/79/1318-2472$01.00/0

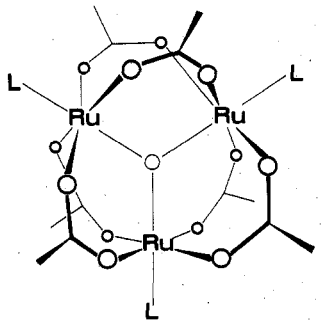

Figure 1. Structure of the cluster unit $[Ru_3O(CH_3CO_2)_6(L)_3]$.[13]

intra- and intercluster interactions, (2) previous mixed-valence systems have been based on single metal redox sites while here the redox sites are delocalized cluster units, and, most importantly, (3) with the extensive reversible redox chemistry of the clusters it is possible to explore variations in cluster–cluster electronic interactions where the only change is in the electron content of the clusters.

Experimental Section

Measurements. Ultraviolet, visible, and very near-infrared spectra were recorded by using Cary Models 14 and 17 and Bausch and Lomb Model 210 spectrophotometers. Spectral deconvolutions were obtained in the range 8500–2000 Å by using the computer program SPECSLV, a local variation of the program BIGAUS for the deconvolution of electronic spectra.[12] Infrared spectra were recorded on a Perkin-Elmer 421 spectrophotometer in KBr pellets, at room temperature. Electrochemical measurements made were vs. the saturated sodium chloride calomel electrode (SSCE) at 25 ± 2 °C and are uncorrected for junction potential effects. The measurements were made by using a PAR Model 173 potentiostat for potential control with a PAR Model 175 universal programmer as a sweep generator for voltammetric experiments. Values of n, where n is the total number of electrons transferred in exhaustive electrolysis at a constant potential, were calculated after measuring the total area under current vs. time curves for a complete electrolysis. Reactions were judged to be complete when the current had fallen below 1% of its initial value. Electrochemical reversibility was determined by cyclic voltammetry, on the basis of the ratio of cathodic to anodic peak currents (i_c/i_a) and the potential separation of the oxidation and reduction peaks (ΔE_p) for each electron-transfer process. All voltammetric measurements were carried out at platinum electrodes. The solutions were deareated by a stream of dry argon or nitrogen when potential scans or electrolyses were carried out at negative potentials. Differential pulse poloragraphy was performed by using a PAR Model 174 polarographic analyzer with a mercury drop electrode.

Materials. Tetra-*n*-butylammonium hexafluorophosphate (TBAH) was recrystallized three times from hot ethanol–water mixtures and vacuum dried at 70 °C for 10 h. Acetonitrile (MCB Spectrograde) was dried over Davidson 4-Å molecular sieves for electrochemical measurements and used without drying for spectral measurements. Water was deionized and then distilled from alkaline permanganate. All other solvents (reagent grade) were used without further purification. The ligands pyrazine (pyr), 4,4′-bipyridine (4,4′-bpy), *trans*-1,2-bis(4-pyridyl)ethylene (BPE), and 1,2-bis(4-pyridyl)ethane (BPA) were obtained commercially and used without further purification. Argon was purified by passing it through a heated column of activated Catalyst R3-11 (Chemical Dynamics Corp.) and then through drying tubes containing Drierite. Elemental analyses were carried out by Galbraith Laboratories, Knoxville, Tenn., PCR, Inc., Gainesville, Fla., and Integral Microanalytical Laboratories, Raleigh, N.C.

Preparations. The "dimeric" series of ligand-bridged clusters discussed here were prepared by reactions between the monodentate ligand clusters $[Ru_3O(OAc)_6(py)_2L](PF_6)$ and the clusters $[Ru_3O(OAc)_6(py)_2(CH_3OH)](PF_6)$ which contain a labile solvent molecule. The syntheses of the two types of clusters were discussed in a previous publication.[8]

$\{[Ru_3O(OAc)_6(py)_2]_2(L)\}(PF_6)_2$ (L = pyr (1a), 4,4′-bpy (1b), BPE (1c), BPA (1d)). In a typical preparation, equimolar amounts of the cluster $[Ru_3O(OAc)_6(py)_2(L)]^+$ and the bis(pyridine)methanol cluster $[Ru_3O(OAc)_6(py)_2(CH_3OH)]^+$ were allowed to react in solution for several days. For example, $[Ru_3O(OAc)_6(py)_2(pyr)](PF_6)$ (161.0 mg, 152.35 mmol) and the bis(pyridine)methanol cluster (154.0 mg, 152.26 mmol) were dissolved in 25 mL of CH_2Cl_2 and stirred for 36 h. The blue solution slowly turned blue-green and deposited a blue-green solid. The solution was filtered, yielding the solid. The solid was recrystallized by dissolving it in the minimum volume of acetonitrile and filtering the solution into stirred diethyl ether. The precipitate which appeared was collected by suction filtration, washed with 2 mL of CH_2Cl_2 and then with Et_2O, and air and vacuum dried (265 mg, 85.5% yield). The 4,4′-bpy and BPE dimeric clusters were prepared similarly and recrystallized by adding petroleum ether slowly into a stirred CH_3CN solution (72 and 75% yields, respectively). The BPA monomer $[Ru_3O(OAc)_6(py)_2(BPA)]^+$ and bis(pyridine)methanol complexes (1:1) were dissolved in CH_2Cl_2 and the solution was stirred for 6 days. No precipitate formed, so the volume was reduced and petroleum ether added dropwise to produce a precipitate. After collection and air and vacuum drying, the complex was obtained in 91% yield. Anal. Calcd for **1a** ($C_{48}H_{60}N_6O_{26}Ru_6P_2F_{12}$): C, 28.35; H, 2.97; N, 4.13. Found: C, 28.27; H, 2.97; N, 4.08. Calcd for **1b** ($C_{54}H_{64}N_6O_{26}Ru_3F_{12}$): C, 30.75; H, 3.06; N, 3.98. Found: C, 30.61; H, 3.13; N, 3.89. Calcd for **1c** ($C_{56}H_{66}N_6O_{26}Ru_6P_2F_{12}$): C, 31.50; H, 3.12; N, 3.94. Found: C, 31.32; H, 3.02; N, 3.91. Calcd for **1d** ($C_{56}H_{68}N_6O_{26}Ru_6P_2F_{12}$): C, 31.47; H, 3.21; N, 3.93. Found: C, 31.38; H, 3.20; N, 3.89.

$[Ru_3O(OAc)_6(py)_2]_2(pyr)$ (2). The reduced pyrazine-bridged dimer was obtained by chemical reduction of the 2+ dimeric cluster. $\{[Ru_3O(OAc)_6(py)_2]_2(pyr)\}(PF_6)_2$ (150 mg) was dissolved in 25 mL of acetonitrile. Several drops of dilute hydrazine (5–10%) were added to the blue solution. The color turned purple and the solution became murky. Methanol (25 mL) was added to the solution, and after 30 min of stirring, the precipitated product was collected. It was washed with methanol and ethyl ether and then air- and vacuum-dried. Anal. Calcd for $C_{48}H_{60}N_6O_{26}Ru_6$: C, 33.07; H, 3.47; N, 4.82. Found: C, 32.90; H, 3.64; N, 4.84.

$\{[Ru_3O(OAc)_6(py)_2]_2(pyr)\}(PF_6)$ (3). The mixed-valence salt was prepared by dissolving equimolar amounts of $\{[Ru_3O(OAc)_6(py)_2]_2(pyr)\}(PF_6)_2$ and $[Ru_3O(OAc)_6(py)_2]_2(pyr)$ in dichloromethane. Solid samples were prepared by precipitation with ethyl ether and then collected and air-dried.

$\{[Ru_3O(OAc)_6(py)_2]_2(pyr)\}(PF_6)_4$ (4). The doubly oxidized dimer was isolated by dissolving the starting complex, $\{[Ru_3O(OAc)_6(py)_2]_2(pyr)\}(PF_6)_2$, in a minimum amount of 0.1 M TBAH/CH_2Cl_2 and oxidizing electrochemically at 1.20 V vs. the SSCE until the current died. The complex, which fell out of solution, was collected by suction filtration, washed with CH_2Cl_2, and air- and vacuum-dried. Anal. Calcd for $C_{48}H_{60}N_6O_{26}Ru_6P_4F_{24}$: C, 24.82; H, 2.60; N, 3.62. Found: C, 24.67; H, 3.83; N, 3.77.

Results

Preparations. We earlier reported the background details of a synthetic procedure which provides a convenient route to dimeric cluster systems where the two cluster units are linked by dibasic N-heterocyclic ligands like pyrazine.[8,9] As used here the procedure exploits the lability of the methanol group in $[Ru_3O(OAc)_6(py)_2(CH_3OH)]^+$, first in the preparation of clusters like $[Ru_3O(OAc)_6(py)_2(pyr)]^+$ (eq 1), which are

$$[Ru_3O(OAc)_6(py)_2(CH_3OH)]^+ + pyr \rightarrow [Ru_3O(OAc)_6(py)_2(pyr)]^+ + CH_3OH \quad (1)$$

themselves ligands. When allowed to react with equimolar amounts of $[Ru_3O(OAc)_6(py)_2(CH_3OH)]^+$ they lead to the desired dimers (eq 2). The same two reactions have been

$$[Ru_3O(OAc)_6(py)_2(pyr)]^+ + [Ru_3O(OAc)_6(py)_2(CH_3OH)]^+ \rightarrow [(py)_2Ru_3O(OAc)_6(pyr)Ru_3O(OAc)_6(py)_2]^{2+} + CH_3OH \quad (2)$$

carried out by using the ligands 4,4′-bpy, BPE, and BPA. Oxidized and reduced forms of the dimers are readily obtainable by chemical or electrochemical oxidation or reduction. Solutions containing mixed-valence cluster dimers like $[(py)_2Ru_3O(OAc)_6(pyr)Ru_3O(OAc)_6(py)_2]^+$ can be prepared

Table I. Reduction Potential Data for the Dimeric $[(py)_2Ru_3O(OAc)_6(L)Ru_3O(OAc)_6(py)_2]^{2+}$ ($Ru_3O(L)Ru_3O^{2+}$) and Related Monomeric $[Ru_3O(OAc)_6(py)_2(L)]^+$ ($Ru_3O(L)^+$) Clusters in 0.1 M $[N(n\text{-}C_4H_9)_4](PF_6)$–$CH_3CN$[a]

	$E_{1/2}$, V vs. the SSCE[b] (ΔE_p)[c]				
cluster	1	2	3	4	5
$[Ru_3O(pyr)Ru_3O]^{2+}$	2.05 (90)	1.07 (90)	+0.09 (60)	−1.10 (60)	−1.88 (100)
			−0.01 (60)	−1.37 (60)	
$[Ru_3O(pyr)]^+$	2.03	1.04	0.00	−1.20	−1.88
$[Ru_3O(4,4'\text{-bpy})Ru_3O]^{2+}$	1.98 (90)	1.02 (85)	−0.04 (80)	−1.29 (120)	−1.82 (80)
$[Ru_3O(4,4'\text{-bpy})]^+$	1.98	1.00	−0.06	−1.29	−1.83
$[Ru_3O(BPE)Ru_3O]^{2+}$	1.96 (90)	1.00 (70)	−0.05 (66)	−1.28 (100)	−1.68 (80)
$[Ru_3O(BPE)]^+$	1.96	0.99	0.05	−1.28	−1.67
$[Ru_3O(BPA)Ru_3O]^{2+}$	1.97 (80)	0.99 (60)	−0.07 (62)	−1.34 (60)	
$[Ru_3O(BPA)]^+$	1.95	1.00	0.06	−1.34	

[a] At 22 ± 2 °C. [b] $E_{1/2}$ values were calculated as the average of the anodic and cathodic peak potentials. The scan rate was 200 mV/s. SSCE is the saturated sodium chloride calomel electrode. [c] ΔE_p is the difference in anodic and cathodic peak potentials.

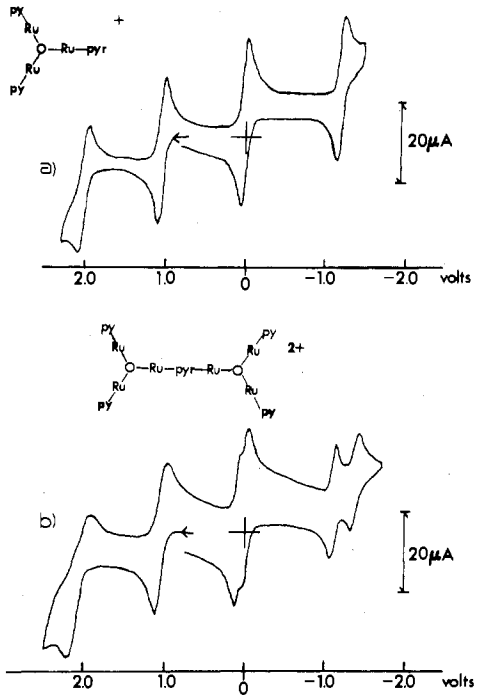

Figure 2. Cyclic voltammograms of $[Ru_3O(OAc)_6(py)_2(pyr)]^+$ (~1 mM) and $[(py)_2Ru_3O(OAc)_6(pyr)Ru_3O(OAc)_6(py)_2]^{2+}$ at room temperature in 0.1 M TBAH–CH_3CN. The concentration of the cluster dimer is approximately half that of the monomeric cluster.

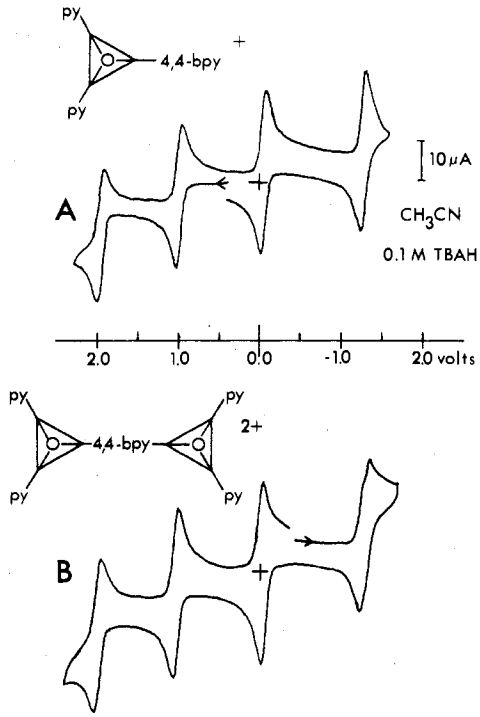

Figure 3. Cyclic voltammograms of $[Ru_3O(OAc)_6(py)_2(4,4'\text{-bpy})]^+$ (~1 mM) and $[(py)_2Ru_3O(OAc)_6(4,4'\text{-bpy})Ru_3O(OAc)_6(py)_2]^{2+}$ at room temperature in 0.1 M TBAH–CH_3CN. The concentration of the dimer is approximately half that of the monomeric cluster.

by simply mixing together solutions containing the corresponding 0 and 2+ dimers.

Electrochemistry. The redox properties of the 2+ dimeric clusters $[(py)_2Ru_3O(OAc)_6(L)Ru_3O(OAc)_6(py)_2]^{2+}$ (L = pyr, 4,4′-bpy, BPE, BPA) were studied by using cyclic voltammetry, coulometry, and in some cases differential pulse polarography. The results of the electrochemical experiments are summarized in Table I, along with data for the clusters $[Ru_3O(OAc)_6(py)_2(L)]^+$ which were reported previously.[8] Cyclic voltammograms for $[(py)_2Ru_3O(OAc)_6(pyr)Ru_3O(OAc)_6(py)_2]^+$ and for the monomer $[Ru_3O(OAc)_6(py)_2(pyr)]^+$ are shown in Figure 2, while Figure 3 compares the cyclic voltammograms for the dimeric and monomeric 4,4′-bpy complexes. The data in Table I are reported as $E_{1/2}$ values for the series of waves (Figures 2 and 3) which occur from ~+2.0 to −2.0 V vs. the saturated sodium calomel electrode (SSCE). For the monomeric clusters, the $E_{1/2}$ values are essentially reduction potentials except for a usually small diffusion coefficient term for the series of one-electron couples $[Ru_3O(OAc)_6(py)_2(L)]^{3+/2+}$, $[Ru_3O(OAc)_6(py)_2(L)]^{2+/+}$, $[Ru_3O(OAc)_6(py)_2(L)]^{+/0}$, $[Ru_3O(OAc)_6(py)_2(L)]^{0/-}$, and $[Ru_3O(OAc)_6(py)_2(L)]^{-/2-}$ as previously reported.[8] The pattern of voltammetric waves for the dimeric clusters is qualitatively similar to the monomers except for the pyrazine- and 4,4′-bipyridine-bridged dimers in the cathodic region (Figures 2 and 3). However, for the dimeric clusters, the peak separations ($\Delta E_p = E_{p,a} - E_{p,c}$) are noticeably larger (80–90 mV compared to 60 mV in the monomers) and the peak currents are approximately doubled (for equimolar solutions). For the dimers, the wave shapes indicate that two slightly split one-electron-transfer processes occur at potentials which are sufficiently close to be unresolvable by cyclic voltammetry, e.g., eq 3 and 4. The situation is analogous to that found for

$$[(py)_2Ru_3O(OAc)_6(pyr)Ru_3O(OAc)_6(py)_2]^{4+} + e^- \rightarrow [(py)_2Ru_3O(OAc)_6(pyr)Ru_3O(OAc)_6(py)_2]^{3+} \quad (3)$$

$$[(py)_2Ru_3O(OAc)_6(pyr)Ru_3O(OAc)_6(py)_2]^{3+} + e^- \rightarrow [(py)_2Ru_3O(OAc)_6(pyr)Ru_3O(OAc)_6(py)_2]^{2+} \quad (4)$$

dimers like $[(bpy)_2ClRu(4,4'\text{-bpy})RuCl(bpy)_2]^{2+}$ (bpy is 2,2′-bipyridine) where the two one-electron oxidations at the Ru(II) sites are also unresolvable by cyclic voltammetry.[14] In both the cluster and Ru–bpy dimers, a slight difference in potential is expected for the two one-electron processes on the basis of electrostatic effects.[1d,3a]

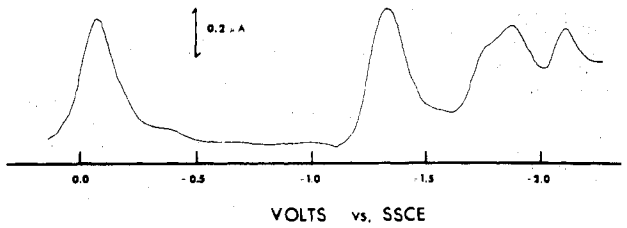

Figure 4. Differential pulse polarogram of $\{[Ru_3O(OAc)_6(py)_2]_2$-$(4,4'\text{-bpy})\}^{2+}$ (~1 mM) in 0.1 M TBAH–CH_3CN.

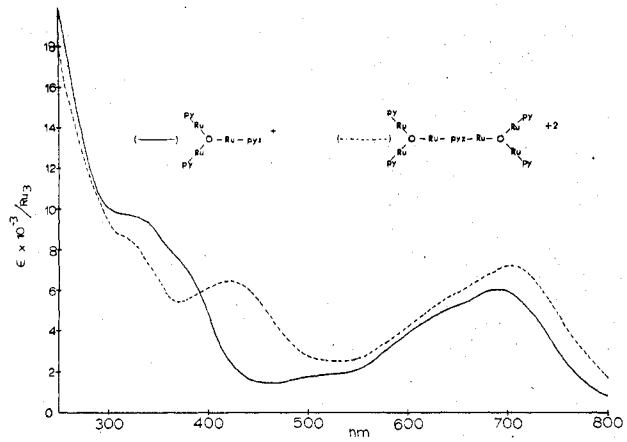

Figure 5. UV–visible absorption spectra of $[Ru_3O(OAc)_6(py)_2(pyr)]^+$ and $[(py)_2Ru_3O(OAc)_6(pyr)Ru_3O(OAc)_6(py)_2]^{2+}$ as PF_6^- salts in CH_2Cl_2 from 250 to 800 nm.

For the pyrazine-bridged dimer, the differences in potential between the $[(py)_2Ru_3O(OAc)_6(pyr)Ru_3O(OAc)_6(py)_2]^{2+/+}$ and $[(py)_2Ru_3O(OAc)_6(pyr)Ru_3O(OAc)_6(py)_2]^{+/0}$ couples is sufficient that two one-electron waves appear, separated by $\Delta E_{1/2}$ = 140 mV. The effect is even more pronounced ($\Delta E_{1/2}$ = 270 mV) for the $[(py)_2Ru_3O(OAc)_6(pyr)Ru_3O(OAc)_6$-$(py)_2]^{0/-}$ and $[(py)_2Ru_3O(OAc)_6(pyr)Ru_3O(OAc)_6(py)_2]^{-/2-}$ couples, where the electron content of the individual cluster sites is greater. For the pyrazine-bridged dimer, an equilibrium constant of 225 (at 22 ± 2 °C) can be calculated for the comproportionation equilibrium in eq 5 by using the $E_{1/2}$ values for the 2+/1+ and +/0 couples.

$$[(py)_2Ru_3O(OAc)_6(pyr)Ru_3O(OAc)_6(py)_2]^{2+} + [(py)_2Ru_3O(OAc)_6(pyr)Ru_3O(OAc)_6(py)_2]^0 \rightleftharpoons 2[(py)_2Ru_3(OAc)_6(pyr)Ru_3O(OAc)_6(py)_2]^+ \quad (5)$$

The redox properties of the dimer $[(py)_2Ru_3O(OAc)_6$-$(4,4'\text{-bpy})Ru_3O(OAc)_6(py)_2]^{2+}$ were studied at strongly reducing potentials by differential pulse polarography, using a mercury drop electrode. Figure 4 shows the differential polarogram for the dimer. The peaks at −0.07 and −1.33 V correspond to waves 3 and 4 in Table I. Below −1.5 V, a shoulder and two distinct peaks appear at ca. −1.78, −1.87, and −2.11 V, respectively. Qualitatively, the peaks correspond to three one-electron-transfer processes. One of the waves is no doubt a ligand-based reduction since similar waves are observed in the pyrazine and BPE dimers and monomers.[8] The remaining two waves appear to be resolvable one-electron reductions at the two cluster sites.

Ultraviolet–Visible Spectra. The UV–visible spectra of the pyrazine-bridged 2+ dimer and the 1+ monomer are shown in Figure 5 and the spectra of the BPA 2+ dimer and 1+ monomer are shown in Figure 6. In Table II a summary is given of the important features of the spectra for the series of 2+ dimers $[(py)_2Ru_3O(OAc)_6(L)Ru_3O(OAc)_6(py)_2]^{2+}$ (L = pyr, 4,4′-bpy, BPE, BPA) and their corresponding 1+ monomers. Also included are data for the reduced pyrazine complexes $[(py)_2Ru_3O(OAc)_6(pyr)Ru_3O(OAc)_6(py)_2]^0$ and $[Ru_3O(OAc)_6(py)_2(pyr)]^0$ and the oxidized clusters $[(py)_2Ru_3O(OAc)_6(pyr)Ru_3O(OAc)_6(py)_2]^{4+}$ and $[Ru_3O$-$(OAc)_6(py)_2(pyr)]^{2+}$. Molar extinction coefficients are given in Table II on a per cluster basis in order to facilitate comparisons between the monomers and dimers.

Table II. Ultraviolet–Visible Spectral Results in CH_2Cl_2

ligand	$[(py)_2Ru_3$-$O(OAc)_6(L)]^{n+}$ λ_{max}, nm (ϵ)	$[(py)_2Ru_3O(OAc)_6$-$(L)Ru_3O(OAc)_6$-$(py)_2]^{2n+}$ λ_{max}, nm (ϵ per cluster)
BPA (n = 1)	692 (6100)	693 (5900)
	325 sh (11000)	325 sh (10650)
	275 sh (15150)	275 sh (14400)
	242 (23800)	241 (22300)
BPE (n = 1)	693 (6331)	694 (6771)
	325 sh (18700)	325 sh (24350)
	291 (32200)	300 (31000)
4,4′-bpy (n = 1)	694 (6400)	696 (6430)
		375 sh (7640)
	325 sh (12300)	325 sh (10550)
	244 (32580)	243 (27700)
pyr (n = 1)	692 (6200)	704 (7265)
		419 (6450)
	325 sh (9560)	325 sh (8320)
	243 (21800)	241 (21450)
pyr (n = 0)	910 (10200)	980 (10700)
	432 (8870)	528 (8450)
	393 (9730)	383 (8650)
	240 (25175)	
pyr (n = 2)[a]	775 (4530)	790 (5700)
	575 (3570)	575 (4200)
	313 (13400)	318 (13050)
	256 (20500)	255 (18500)

[a] In CH_3CN.

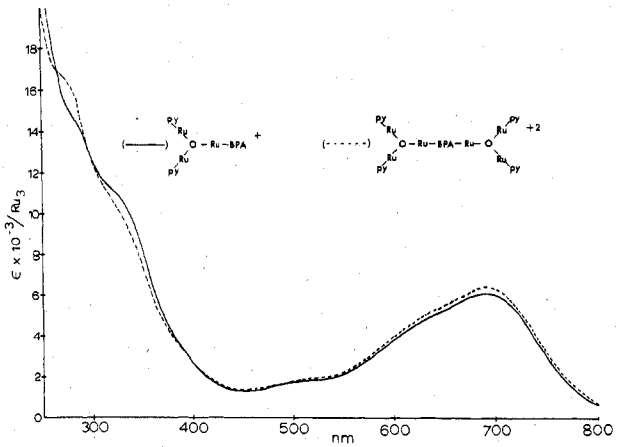

Figure 6. UV–visible absorption spectra of $[Ru_3O(OAc)_6(py)_2(BPA)]^+$ and $[(py)_2Ru_3O(OAc)_6(BPA)Ru_3O(OAc)_6(py)_2]^{2+}$ as PF_6^- salts in CH_2Cl_2 from 250 to 800 nm.

The nearly identical spectra for the BPA monomer and dimer (Figure 6) show that the spectra of the separate clusters, which are dominated by intracluster transitions,[8] are unperturbed in the dimer. On the other hand, there are significant differences between the pyr monomer and dimer spectra (Figure 5) and the differences will be discussed in a later section.

As pointed out previously, the spectra of the individual clusters $[Ru_3O(OAc)_6(py)_2(L)]^{2+/+/0}$ consist of broad, structured absorptions which can be resolved into a series of bands.[8] A spectral deconvolution of the spectrum of the dimer $[(py)_2Ru_3O(OAc)_6(pyr)Ru_3O(OAc)_6(py)_2]^{2+}$ using the program SPECSOLV[12] was obtained. The results for both the 2+ dimer and $[Ru_3O(OAc)_6(py)_2(pyr)]^+$ are summarized in Table III. The most notable difference between the monomer and dimer spectra occurs for the fourth transition listed, which

Table III. Resolved Spectral Bands for the Clusters $[Ru_3O(OAc)_6(py)_2(pyr)]^+$ and $[(py)_2Ru_3O(OAc)_6(pyr)Ru_3O(OAc)_6(py)_2]^{2+}$ in CH_2Cl_2

$[Ru_3O(OAc)_6(py)_2(pyr)]^+$ $10^{-3}\lambda_{max}$, cm^{-1} ($10^2 f$ per cluster)[a,b]	$[(py)_2RuO(OAc)_6(pyr)Ru_3O(OAc)_6(py)_2]^{2+}$ $10^{-3}\lambda_{max}$, cm^{-1} ($10^2 f$)[a]
14.3 (6.5)	14.2 (9.6)
16.6 (3.4)	16.8 (3.3)
19.6 (1.9)	19.1 (1.0)
26.0 (2.0)	23.1 (13)
30.6 (48)	31.6 (40)
35.5 (2.3)	36.0 (4.8)
41.3 (68)	41.8 (68)

[a] f = oscillator strength. The data were calculated from the measured spectra using the spectral deconvolution program SPECSOLV.[12] [b] f values for the dimers are reported per cluster unit for ease of comparison with the corresponding monomers.

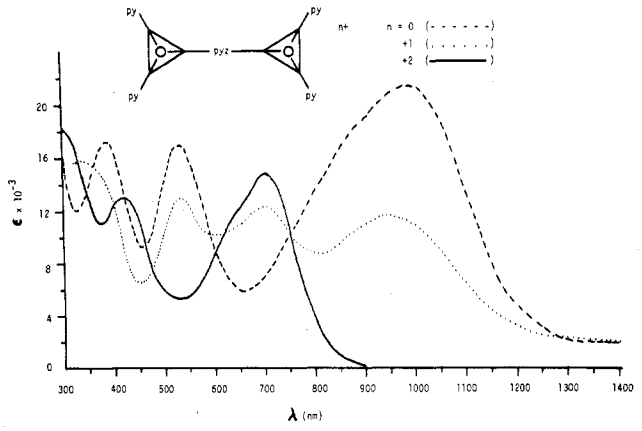

Figure 7. UV–visible absorption spectra for $[(py)_2Ru_3O(OAc)_6(pyr)Ru_3O(OAc)_6(py)_2]^{n+}$ (n = 0, 1, 2) in CH_2Cl_2 from 300 to 1400 nm.

shifts in energy from 2.6 to 2.31 μm^{-1} and increases in intensity by a factor of 6.5.

In Figure 7 are shown the UV–visible–near-infrared (near-IR) spectra for the 0, 1+, and 2+ cluster dimers $[(py)_2Ru_3O(OAc)_6(pyr)Ru_3O(OAc)_6(py)_2]^{n+}$ (n = 0, 1+, 2+). The spectrum of the 1+ dimer, which is a "mixed-valence" case with regard to the two cluster sites, has been corrected for the comproportionation equilibrium in eq 5.

The spectrum of the 1+ ion is to a first approximation the average of the sum of the 1+ and 2+ dimers. Of special interest to us was the possible appearance of a low-energy absorption band in the near-IR for the 1+ dimer. Unfortunately, much of the spectral region of interest is partly obscured by low-energy tailing of the band at λ_{max} 980 nm for the Ru_3O^0 cluster site in the dimer. However, close inspection of Figure 7 shows that the spectrum of the 1+ dimer rises into the near-IR. A difference spectrum for the 1+ dimer was calculated by assuming its spectrum was the sum of half the absorbance of the 2+ dimer at the same concentration and half the absorbance of the 0 dimer at the same concentration. The difference spectrum obtained in this way can only be approximate since it is expected that at least slight deviations from the averaged sum of the 0 and 2+ spectra will exist. Nevertheless, the procedure does provide evidence for a low-energy band for the 1+ dimer at λ_{max} 1000–1400 nm (ϵ 1000–1200). A difference spectrum for the 3+ mixed-valence dimer $[(py)_2Ru_3O(OAc)_6(pyr)Ru_3O(OAc)_6(py)_2]^{3+}$ calculated as the average of the spectra of the 2+ and 4+ dimers also gave evidence for a low-energy band at λ_{max} 1000–1300 nm ($\epsilon \sim 500$) which was less well defined.

ESCA. Ru $3d_{5/2}$ binding energies for the monomer clusters $[Ru_3O(OAc)_6(py)_3]$ and $[Ru_3O(OAc)_6(py)_3]^+$ and for the dimer $[(py)_2Ru_3O(OAc)_6(pyr)Ru_3O(OAc)_6(py)_2]^+$ are given in Table IV. The effect of the gain or loss of electrons from the clusters was discussed previously in terms of a delocalized, molecular orbital model.[8] The obvious result to report here is that the mixed-valence dimer shows two binding energies, one of which is approximately that of the reduced monomer and the other that of the oxidized monomer.

Table IV. Ru $3d_{5/2}$ Binding Energy Data vs. C 1s at 284.4 eV[a]

compd	eV
$[Ru_3O(CH_3CO_2)_6(py)_3]$	279.3
$[Ru_3O(CH_3CO_2)_6(py)_3](PF_6)$	280.4
$\{[Ru_3O(CH_3CO_2)_6(py)_2]_2(pyr)\}(PF_6)$	279.4
	280.3

[a] As solid samples

Infrared Spectra. The solid-state infrared spectra (KBr pellets) of the dimers $[(py)_2Ru_3O(OAc)_6(pyr)Ru_3O(OAc)_6(py)_2]^{0,2+}$ are very similar to the spectra reported earlier[8] for the 0 and 1+ clusters, $[Ru_3O(OAc)_6(py)_2(pyr)]^{0,+}$, respectively. There are only slight differences between the spectra of the 0 and 1+ clusters. The spectrum of the mixed-valence dimer $[(py)_2Ru_3O(OAc)_6(pyr)Ru_3O(OAc)_6(py)_2]^+$ is essentially the average of the spectra of the 0 and 2+ dimers. There are two features in the spectrum of the 1+ ion which suggest that there are discrete $[Ru_3O]^0$ and $[Ru_3O]^+$ sites. Bands which can be assigned to $\nu_{as}(CO_2^-)$ for the bridging carboxylate groups appear at 1555 and 1585 cm^{-1} for the 0 dimer and at 1541 cm^{-1} (and 1609 cm^{-1}) for the 2+ dimer. In the mixed-valence dimer, the intensity of the higher energy band (at 1587 cm^{-1}) is noticeably enhanced. In the dimers $[(bpy)_2ClRu(pyr)RuCl(bpy)_2]^{2+/3+/4+}$, a band assignable to ν_{sym}(pyr) appears at 1599 cm^{-1} but only for the mixed-valence 3+ ion. The appearance of the band has been taken as evidence for discrete Ru(II) and Ru(III) sites on the infrared time scale.[3a] If the origin of the enhancement in intensity of the band at 1587 cm^{-1} for the 1+ dimer is because of the appearance of a ν_{sym}(pyr) stretching mode, it would suggest that there are localized $[Ru_3O]^+$ and $[Ru_3O]^0$ sites in the mixed-valence cluster dimer. It is also worth noting that a band of unknown origin appears at 560 cm^{-1} for $[Ru_3O(OAc)_6(py)_3]^+$, at 554 cm^{-1} for $[Ru_3O(OAc)_6(py)_2(pyr)]^+$, and at 559 cm^{-1} for the 2+ dimer. The band does not appear either for $[Ru_3O(OAc)_6(py)_3]^0$ or for the neutral dimer. However, in the mixed-valence 1+ dimer a band does appear at 555 cm^{-1} which has a relative intensity which is roughly half that of near-lying bands. The appearance of this low-energy band also suggests the presence of discrete $[Ru_3O]^+$ and $[Ru_3O]^0$ sites in the mixed-valence cluster dimer.

Discussion

In Figure 8 is shown a schematic molecular orbital diagram which has been applied to the π-electronic structures of the clusters, $[Ru_3O(OAc)_6(L)_3]^{m+}$ (m = 2, 1, 0). The diagram is based on the earlier work of Cotton and Norman[13] and the results of spectral studies on the 2+, 1+, and 0 cluster systems. The redox and spectral properties of the clusters can be understood in terms of a series of delocalized, cluster-based π-bonding, π-nonbonding, and π-antibonding levels which are largely Ru–Ru and Ru–O–Ru in character. In the neutral clusters, $[Ru_3O(OAc)_6(L)_3]^0$, the A_2' level, which is metal–metal antibonding in character, is filled. Oxidation to the 1+ and 2+ clusters involves stepwise loss of electrons from the A_2' level. Loss of a third electron to give the 3+ cluster occurs at the degenerate E'' levels which are Ru–O–Ru nonbonding in character. Reduction of the neutral cluster occurs first at the vacant Ru–O–Ru antibonding A_2'' level, followed closely by a reduction based on π^* ligand levels to give the 2– clusters.

By use of the MO scheme in Figure 8, it is possible to understand the spectral and redox properties expected for

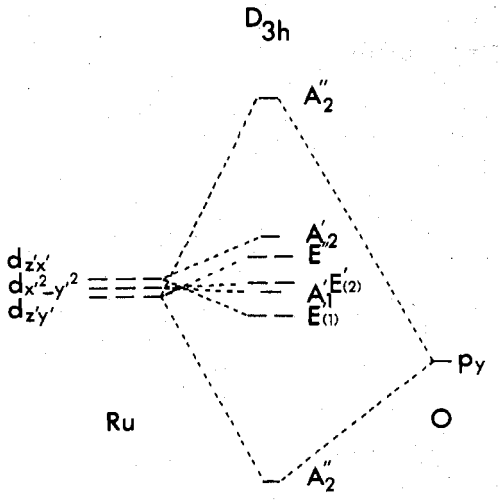

Figure 8. Qualitative molecular orbital scheme for the cluster π system in D_{3h} symmetry.

isolated, noninteracting cluster sites in the ligand-bridged cluster dimers. Deviations from the properties expected for isolated clusters will arise because of cluster–cluster interactions across the bridging ligands. In addition to through-space electrostatic effects,[1a,d] an orbital pathway for electronic interactions between clusters exists on the basis of the π or π^* systems of the bridging ligands, pyr, 4,4-bpy, and BPE. Optimal mixing can occur between cluster A_2'' or E'' orbitals and π or π^* (ligand) orbitals if the plane of the ligand is parallel to the plane of the cluster and with A_2' or E' cluster orbitals if the plane of the ligand is perpendicular to the plane of the cluster. The importance of such mixing is seen in the appearance of what appear to be cluster to ligand charge transfer (CLCT) bands in the absorption spectra of the neutral clusters $[Ru_3O(CH_3CO_2)_6(py)_2(L)]$. It is especially notable that a new absorption band appears for the case where L is pyrazine and that the origin of the band is probably a relatively low-lying cluster to pyrazine CT transition.

As the electron content of the clusters increases, the extent of cluster–π^*(ligand) mixing will increase as will cluster–cluster interactions by cluster–π^*(ligand)–cluster mixing. When the electron content of the clusters is high, the A_2'' (Ru–O–Ru *antibonding*) orbital is occupied. The A_2'' orbital is strongly antibonding with regard to the Ru_3O core and is largely Ru in character. It should interact strongly with π^*(ligand) orbitals since it is directed away from the Ru_3O core along the three terminal Ru–ligand axes (Figure 1) and energetically it is near the π^*(ligand) levels.

Spectral and Redox Properties. Cyclic voltammograms for the monomers $[Ru_3O(CH_3CO_2)_6(py)_2(L)]^+$ and related dimers $[(py)_2RuO(CH_3CO_2)_6(L)Ru_3O(CH_3CO_2)_6(py)_2]^{2+}$ (L = 4,4′-bpy, BPE, BPA) are nearly identical except for subtle changes in the wave shapes and small increases in ΔE_p values. At least slight differences in $E_{1/2}$ values for oxidation or reduction of the two cluster sites (e.g., eq 6) are expected even

$$Ru^+{}_3O\text{–}L\text{–}Ru^0{}_3O \underset{-e^-}{\overset{+e^-}{\rightleftharpoons}} Ru^0{}_3O\text{–}L\text{–}Ru^0{}_3O \qquad (6a)$$

$$Ru^+{}_3O\text{–}L\text{–}Ru^+{}_3O \underset{-e^-}{\overset{+e^-}{\rightleftharpoons}} Ru^+{}_3O\text{–}L\text{–}Ru^0{}_3O \qquad (6b)$$

in the absence of significant intracluster electronic interactions.[1a,d,3a] A difference in $E_{1/2}$ values is favored by electrostatic effects,[3a] and the noticeable broadening of the waves in the cyclic voltammograms of the dimers may arise because of slight differences in the $E_{1/2}$ values for the two cluster sites which are irresolvable by cyclic voltammetry.[14] It is also true that in solution, mixed-valence dimers are favored by a factor of 4 with regard to comproportionation equilibria like that in eq 5.[3a]

The cyclic voltammogram for the pyrazine-bridged dimer differs from the other three in that as the electron content of the clusters increases, discrete one-electron waves are observed. $\Delta E_{1/2}$ for the $[Ru_3O(pyr)Ru_3O]^{2+/+}$ and $[Ru_3O(pyr)Ru_3O]^{+/0}$ couples is 0.140 V in the potential region expected for the cluster $Ru_3O^{-+/0}$ couples. $\Delta E_{1/2}$ for the $[Ru_3O(pyr)Ru_3O]^{0/-}$ and $[Ru_3O(pyr)Ru_3O]^{-/2-}$ couples, which occur in the potential region expected for the $Ru_3O^{0/-}$ couples, are considerably larger, 0.270 V.

The same effect has been observed in the dimers $[(bpy)_2ClRu(L)RuCl(bpy)_2]^{2+/3+/4+}$ where a noticeable peak splitting is observed only for L = pyrazine, and from the properties of the IT band for the 3+, mixed-valence ion, it has been concluded that there is an appreciable electronic coupling between redox sites (~1 kcal/mol) only across pyrazine as the bridging ligand.[3a] The orbital mechanism for Ru–Ru interaction may involve $d\pi(Ru(II))$–$\pi^*(pyr)$ mixing which extends the d (Ru(II)) wave functions to the Ru(III) site or simply the closer proximity of the two Ru sites,[16] but in any case pyrazine promotes a stronger interaction than do the other three ligands.

The contribution to $\Delta E_{1/2}$ from electrostatic effects should be independent of the charge types involved.[3a] Since the splittings between waves for the $Ru_3O(pyr)^{2+/+}$ and $Ru_3O(pyr)^{3+/2+}$ couples for the dimer are irresolvable by cyclic voltammetry, the origin of the splittings for the $Ru_3O(pyr)^{+/0}$ and $Ru_3O(pyr)^{0/-}$ couples cannot be solely electrostatic in nature. This suggests that electronic delocalization between clusters may be an important feature in the mixed-valence dimer $[(py)_2Ru_3O(OAc)_6(pyr)Ru_3O(OAc)_6py]^+$ and even more so in the dimer $[(py)_2Ru_3O(OAc)_6(pyr)Ru_3O(OAc)_6(py)_2]^-$. As discussed earlier, cluster–cluster electronic interactions are expected to be the greatest for the 1– mixed-valence ion since the additional electron is added to the antibonding Ru–O–Ru antibonding A_2'' orbital. The importance of cluster electron content on the extent of intercluster interaction is also shown by the pulse polarography experiment on the dimer $[(py)_2Ru_3O(CH_3CO_2)_6(4,4'\text{-bpy})Ru_3O(CH_3CO_2)_6(py)_2]^{2+}$. There, clear evidence was obtained for separated, one-electron $(Ru_3O)^{0/-}$ couples suggesting an observable interaction even across 4,4′-bipyridine as the bridging ligand.

The UV–visible spectra of the monomeric 2+, 1+, and 0 clusters are dominated in the visible by intracluster transitions from filled Ru–Ru and Ru–O–Ru cluster levels to the empty A_2'' level. In the UV the spectra are dominated by $\pi^* \leftarrow \pi$ transitions of the organic ligands and to a lesser degree by cluster–ligand CLCT transitions.

All of the transitions are somewhat affected by dimerization, but for the 4,4′-bpy, BPE, and BPA dimers the spectral changes are slight and they only become pronounced for the pyrazine-bridged dimers. For the 2+ dimer, a distinct absorption band appears at λ_{max} 419 nm (2.38 μm^{-1}) which is apparently a cluster to pyrazine CT transition which has been red-shifted and is far more intense than the cluster to pyrazine CT band in $[Ru_3O(OAc)_6(py)_2(pyr)]^+$ (λ_{max} 385 nm). A similar effect is observed in comparing monomer and dimer spectra for related complexes of $Ru^{II}(NH_3)_5$–[4,5] and $Ru^{II}(bpy)_2Cl$–,[3a] but the intensity enhancement is far more dramatic in the cluster dimers. In the dimer $[(py)_2Ru_3O(OAc)_6(pyr)Ru_3O(OAc)_6(py)_2]^0$, a band appears at 528 nm (ϵ 8400) which is presumably a cluster to pyr CT band. The band is significantly red-shifted compared to the band at ~472 nm in $[Ru_3O(OAc)_6(py)_2(pyr)]^0$ but the lowering in energy is expected because of stabilization of the π^*(pyr) level in the dimer.[5,17]

Slight spectral shifts on dimerization are also observed for the intracluster transitions. The shifts vary somewhat in the dimers $[(py)_2Ru_3O(OAc)_6(pyr)Ru_3O(OAc)_6(py)_2]^{2+/+/0}$, but in general the spectral envelopes shift to lower energy or increase in intensity or both.

In summary, where available, the spectral and redox potential data suggest that the delocalized intramolecular electronic structure of the cluster sites is maintained in the dimers. Relative to the strong electronic coupling within the clusters, intercluster interactions are relatively weak and appear to depend in a significant way on the nature of the bridging ligand and on the electron content of the clusters.

Mixed-Valence Dimers of Trimers. From $E_{1/2}$ values, K for the comproportionation equilibrium in eq 5 is 224 in CH_2Cl_2 at 22 ± 2 °C. Because of the magnitude of the equilibrium constant, solutions containing largely the mixed-valence dimer can be prepared by mixing solutions containing the 2+ and 0 dimers. Electron transfer equilibration is rapid. The mixed-valence dimer can be isolated from solution as a solid PF_6^- salt and the IR spectrum of the solid suggests that it contains the salt $[(py)_2Ru_3O(OAc)_6(pyr)Ru_3O(OAc)_6(py)_2](PF_6)$ rather than a solid-state mixture of the 2+ and 0 dimers.

From our results it appears that the mixed-valence 1+ dimer contains discrete, localized $[Ru_3O]^+$ and $[Ru_3O]^0$ groups. From the ESCA results, two Ru $3d_{5/2}$ peaks are observed at characteristic binding energies expected for $[Ru_3O]^+$ and $[Ru_3O]^0$ sites (Table IV). Although not definitive, the IR spectrum of the solid also suggests that there are localized redox sites. After correcting for the slight amounts of the 2+ and 0 dimers in solution, the electronic spectrum of the 1+ dimer includes absorption envelopes characteristic of $[Ru_3O]^0$ (λ_{max} 950) and $[Ru_3O]^+$ (λ_{max} 700) which are only slightly perturbed in the dimer.

In dimers like $[(NH_3)_5Ru(pyr)Ru(NH_3)_5]^{5+}$ and $[(bpy)_2ClRu(pyr)RuCl(bpy)_2]^{3+}$, low-energy absorption bands are observed in the near-IR which are associated with the mixed-valence nature of the materials.[3-5] The observation of such transitions can be of great value in gaining insight into the extent of electronic coupling between redox sites in the ground state[4,7,18] and in estimating the thermal activation barrier to intramolecular electron transfer.[3b]

As we noted earlier, attempts to find mixed-valence transitions in the cluster dimers is difficult because the intracluster absorption envelopes for the $[Ru_3O]^+$ and $[Ru_3O]^0$ groups tail into the near-IR region. However, the absorption spectrum of the mixed-valence 1+ dimer appears to have some residual absorbance at low energy (Figure 7), and we have investigated difference spectra in this region.

The difference spectra were generated in two ways. One involved assuming that the spectrum of the 1+ dimer consisted of the sum of the spectra of the isolated $[Ru_3O(OAc)_6(py)_2(pyr)]^0$ and 1+ clusters while the other considered the 1+ spectrum as the average of the spectra of the 0 and 2+ dimers. Neither of the assumptions is adequate because, as noted earlier, there are band shifts and intensity enhancements in the dimers when compared to the monomers and the extents of these shifts and enhancements are different for the 0, 1+, and 2+ dimers. However, with either assumption, clear evidence was obtained for a new absorption feature for the mixed-valence dimer in the near-IR. Because of the uncertainties involved, we can only estimate that in CH_2Cl_2 the band λ_{max} is in the region 1200 ± 200 nm with ϵ_{max} probably >1000. Given the evidence for localized, cluster-based redox sites in the mixed-valence dimer, the origin of the band is probably a cluster cluster charge transfer (CCCT) or IT transition (eq 7). The band appears in the same spectral region as the IT band for $[(bpy)_2ClRu(pyr)RuCl(bpy)_2]^{3+}$ [3a] which suggests that as for the bpy ion, the energy of activation for intramolecular electron transfer across the pyrazine bridge is small.

$$[Ru^+{}_3O(pyr)Ru^0{}_3O]^+ \xrightarrow{h\nu} [Ru^0{}_3O(pyr)Ru^+{}_3O]^{+*} \quad (7)$$

We have also investigated the solution spectral properties of the 3+ mixed-valence dimer $[(py)_2Ru_3O(OAc)_6(pyr)Ru_3O(OAc)_6(py)_2]^{3+}$ generated by mixing equimolar amounts of the 4+ and 2+ dimers. Once again, a tailing to low energies was observed compared to the spectra of separate 2+ and 4+ dimers. Difference spectra suggest the presence of a new absorption band for the 3+ dimer in the same region (1000–1300 nm) as for the 1+ dimer. Assuming that the constant for the comproportionation equilibrium in eq 8 is ≥4 allows the value ϵ_{max} <400 to be estimated.

$$[Ru_3O(pyr)Ru_3O]^{4+} + [Ru_3O(pyr)Ru_3O]^{2+} \rightleftharpoons 2[Ru_3O(pyr)Ru_3O]^{3+} \quad (8)$$

Given the evidence for localized cluster sites in the 1+ dimer and the similarity in the low-energy bands for the 1+ and 3+ mixed-valence dimers, it seems reasonable to conclude the 3+ dimer is also a localized case and that the near-IR band is a CCCT or IT transition between $[Ru_3O]^{2+}$ and $[Ru_3O]^+$ cluster sites (eq 9).

$$[Ru^{2+}{}_3O(pyr)Ru^+{}_3O]^{3+} \xrightarrow{h\nu} [Ru^+{}_3O(pyr)Ru^{2+}{}_3O]^{3+*} \quad (9)$$

We have made no attempt to search for new low-energy bands for the 1+ or 3+ dimers where the bridging ligand is 4,4′-bpy, BPE, or BPA. Earlier work with the $[(bpy)_2ClRu(L)RuCl(bpy)_2]^{3+}$ dimers has shown that IT bands, where observable, are weaker and are at higher energies than for the L = pyrazine case.[3b,14] IT bands in the cluster dimers, if they exist for the remaining ligands, would be completely obscured by the intramolecular cluster transitions.

In any case, even the qualitative evidence for the appearance of IT bands for the 1+ and 3+ dimers is of interest. The bands are novel in that they involve optical electron transfer between delocalized cluster levels across a bridging ligand rather than electron transfer between single metal sites. In the transition the individual cluster units can be thought of as "super" redox sites in that the redox levels involved include contributions from several metal ions. From the properties of the bands, it appears that the energy of the optical transition and therefore the energy of activation for thermal electron transfer[16,18a] is only slightly affected by the electron content of the donor and acceptor sites. The greater intensity of the IT band for the 1+ dimer is consistent with stronger electronic coupling between clusters in the more electron-rich system.

From the electrochemical evidence for enhanced electronic coupling, the situation may be quite different in the 1− dimer, $[Ru_3O(pyr)Ru_3O]^-$. There, if electronic coupling is sufficiently strong, the two cluster sites could well be vibrationally equivalent and the electronic structure at the clusters significantly perturbed as shown by spectral shifts. Unfortunately, we have not yet been able to obtain reliable optical spectra of the reduced complexes in solution because of their extreme air sensitivity.

Acknowledgment. Acknowledgments are made to the Army Research Office—Durham under Grant No. DAAG29-76-G-0135, to the Materials Research Center of The University of North Carolina under Grant No. DAHC15-73-G9, and to the donors of the Petroleum Research Fund, administered by the American Chemical Society, for support of this research and to Pamela L. Hood, a National Science Foundation Undergraduate Research Program participant, for her efforts in the completion of the work.

Registry No. **1a**, 70766-17-5; **1b**, 70766-14-2; **1c**, 70766-12-0; **1d**, 70766-16-4; **2**, 70812-66-7; **3**, 70879-12-8; **4**, 70879-13-9; $[Ru_3O(OAc)_6(py)_2(4,4'\text{-bpy})](PF_6)$, 67815-42-3; $[Ru_3O(OAc)_6(py)_2(BPE)](PF_6)$, 67815-44-5; $[Ru_3O(OAc)_6(py)_2(BPA)](PF_6)$,

67815-46-7; $[Ru_3O(OAc)_6(py)_2(pyr)](PF_6)$, 67815-40-1; $[Ru_3O(pyr)Ru_3O]^{3+}$, 70812-63-4; $[Ru_3O(OAc)_6(py)_2(CH_3OH)](PF_6)$, 67815-39-8; $[Ru_3O(pyr)Ru_3O]^-$, 70812-64-5; $[Ru_3O(pyr)Ru_3O]^{2-}$, 70812-65-6; $[Ru_3O(4,4'\text{-bpy})Ru_3O]^{3+}$, 70812-71-4; $[Ru_3O(4,4'\text{-bpy})Ru_3O]^+$, 70812-67-8; $[Ru_3O(4,4'\text{-bpy})Ru_3O]^0$, 70812-68-9; $[Ru_3O(4,4'\text{-bpy})Ru_3O]^-$, 70812-69-0; $[Ru_3O(4,4'\text{-bpy})Ru_3O]^{2-}$, 70812-70-3; $[Ru_3O(BPE)Ru_3O]^{3+}$, 70812-75-8; $[Ru_3O(BPE)Ru_3O]^+$, 70850-22-5; $[Ru_3O(BPE)Ru_3O]^0$, 70812-72-5; $[Ru_3O(BPE)Ru_3O]^-$, 70812-73-6; $[Ru_3O(BPE)Ru_3O]^{2-}$, 70812-74-7; $[Ru_3O(BPA)Ru_3O]^{3+}$, 70812-79-2; $[Ru_3O(BPA)Ru_3O]^+$, 70812-76-9; $[Ru_3O(BPA)Ru_3O]^0$, 70812-77-0; $[Ru_3O(BPA)Ru_3O]^-$, 70812-78-1; $[Ru_3O(OAc)_6(py)_2(pyr)]^{2+}$, 67954-61-4; $[Ru_3O(OAc)_6(py)_2(pyr)]^0$, 67951-63-7; $[Ru_3O(CH_3CO_2)_6(py)_3]^0$, 37337-93-2; $[Ru_3O(CH_3CO_2)_6(py)_3](PF_6)$, 67815-38-7.

References and Notes

(1) (a) H. Taube, *Ann. N.Y. Acad. Sci.*, **313**, 481 (1978); (b) T. J. Meyer, *ibid.*, **313**, 496 (1978); (c) *Acc. Chem. Res.*, **11**, 94 (1978); (d) *Adv. Chem. Ser.*, **No. 150**, Chapter 7 (1976); G. M. Brown, R. W. Callahan, E. C. Johnson, T. J. Meyer, and T. R. Weaver, *ACS Symp. Ser.*, **No. 5**, 66 (1975); (e) D. O. Cowan, C. LeVanda, J. Park, and F. Kaufman, *Acc. Chem. Res.*, **6**, 1 (1973).

(2) (a) W. H. Morrison, Jr., and D. N. Hendrickson, *Inorg. Chem.*, **14**, 2331 (1975); (b) R. F. Kirchner, G. H. Love, and U. T. Mueller-Westerhoff, *ibid.*, **15**, 2665 (1976); (c) M. J. Powers and T. J. Meyer, *J. Am. Chem. Soc.*, **100**, 4393 (1978).

(3) (a) R. W. Callahan, F. R. Keene, T. J. Meyer, and D. J. Salmon, *J. Am. Chem. Soc.*, **99**, 1064 (1977); (b) T. J. Meyer, M. J. Powers, D. J. Salmon, and R. W. Callahan, *ibid.*, **98**, 6731 (1976); (c) T. J. Meyer, T. R. Weaver, S. A. Adeyemi, G. M. Brown, R. P. Eckberg, W. E. Hatfield, E. C. Johnson, R. W. Murray, and D. Untereker, *ibid.*, **97**, 3039 (1975).

(4) (a) C. Creutz and H. Taube, *J. Am. Chem. Soc.*, **91**, 3988 (1969); **95**, 1086 (1973); (b) J. K. Beattie, N. S. Hush, and P. R. Taylor, *Inorg. Chem.*, **15**, 992 (1976).

(5) C. Creutz, Ph.D. Dissertation, Stanford University, 1971.

(6) (a) G. M. Tom and H. Taube, *J. Am. Chem. Soc.*, **97**, 5310 (1975); (b) H. Krentzien and H. Taube, *ibid.*, **98**, 6379 (1976); (c) H. Fischer, G. M. Tom, and H. Taube, *ibid.*, **98**, 5512 (1976).

(7) N. Hush, *Chem. Phys.*, **10**, 361 (1975).

(8) J. A. Baumann, S. T. Wilson, T. J. Meyer, D. J. Salmon, and W. E. Hatfield, *Inorg. Chem.*, **17**, 3342 (1978).

(9) T. J. Meyer, S. T. Wilson, R. F. Bondurant, and D. J. Salmon, *J. Am. Chem. Soc.*, **97**, 2285 (1975).

(10) A. Spencer and G. Wilkinson, *J. Chem. Soc., Dalton Trans.*, 1570 (1972).

(11) A. Spencer and G. Wilkinson, *J. Chem. Soc., Dalton Trans.*, 796 (1974).

(12) (a) H. Gold, C. E. Rechsteiner, and R. P. Buck, *Anal. Chem.*, **48**, 1540 (1976); (b) H. Gold, "SPECSOLV-A Generalized Spectral Deconvolution Program", Library Science Series Document LS-301, Research Triangle Park, Triangle Universities Computation Center, 1976.

(13) F. A. Cotton and J. G. Norman, Jr., *Inorg. Chim. Acta*, **6**, 411 (1972).

(14) M. J. Powers, Ph.D. Dissertation, University of North Carolina, Chapel Hill, NC, 1977; M. J. Powers and T. J. Meyer, submitted for publication.

(15) (a) M. J. Powers, R. W. Callahan, and T. J. Meyer, *Inorg. Chem.*, **15**, 1457 (1976); (b) J. N. Murrell and K. J. Laidler, *Trans. Faraday Soc.*, **64**, 371 (1968).

(16) M. J. Powers and T. J. Meyer, *Inorg. Chem.*, **17**, 2155 (1978).

(17) R. W. Callahan, G. M. Brown, and T. J. Meyer, *Inorg. Chem.*, **14**, 1443 (1975).

(18) (a) N. S. Hush, *Prog. Inorg. Chem.*, **8**, 3911 (1967); *Electrochim. Acta*, **13**, 1005 (1968); (b) M. B. Robin and D. Day, *Adv. Inorg. Chem. Radiochem.*, **10**, 247 (1967).

Contribution from the Department of Chemistry, Boston University, Boston, Massachusetts 02215, and Food Engineering Laboratory, U.S. Army Natick Research and Development Command, Natick, Massachusetts 01760

Intramolecular Electron Transfer in the Reaction of Hydroxyl Radicals with (Pyridine)pentaamminecobalt(III) Ion in Aqueous Solution[1]

MORTON Z. HOFFMAN,*[2a] DAVID W. KIMMEL,[2a] and MICHAEL G. SIMIC[2b]

Received February 5, 1979

The reaction of radiation-generated OH radicals with $Co(NH_3)_5py^{3+}$ in aqueous solution to form $Co^{2+}(aq)$ serves as a model of induced electron transfer. The yield of $Co^{2+}(aq)$ formation is dependent upon the radiation dose rate, pH, and the gas used to purge the solutions (N_2O, N_2, O_2). The initial reaction of OH with $Co(NH_3)_5py^{3+}$ ($k = 6.5 \times 10^8$ M^{-1} s^{-1}) involves addition of the radical to the aromatic ligand; pulse radiolysis reveals the absorption spectrum of this Co(III)-coordinated ligand-radical species (I) (λ_{max} 325 nm, ϵ_{max} 1.7×10^3 M^{-1} cm^{-1}) and shows that it is readily scavenged by O_2 ($k = 4.4 \times 10^8$ M^{-1} s^{-1}). Species I is converted ($k = 8.5 \times 10^3$ s^{-1}) into a similarly coordinated ligand-radical species (II), possibly via solvent-assisted ligand modification. Species II undergoes bimolecular decay ($2k = 3.6 \times 10^5$ M^{-1} s^{-1}) in competition with a deprotonation reaction with OH^- ($k = 1.8 \times 10^8$ M^{-1} s^{-1}) and ligand-to-metal intramolecular electron transfer to form $Co^{2+}(aq)$ ($k = 2.3 \times 10^{-2}$ s^{-1}). The deprotonated coordinated ligand radical undergoes bimolecular decay ($2k = 3.8 \times 10^7$ M^{-1} s^{-1}) in competition with intramolecular electron transfer to form $Co^{2+}(aq)$ ($k = 1.1 \times 10^1$ s^{-1}). A comparison of these intramolecular electron rate constants is made with those that have been obtained for other ligand radicals coordinated to Co(III) centers.

Introduction

Induced electron transfer, wherein the interaction of a one-electron oxidant with a metal complex leads to the formation of the one-electron-reduced metal center, remains an intriguing mechanistic problem.[3] Among the systems studied are a series of $Co^{III}(NH_3)_5X$ complexes where X = carbinol pyridine;[4] oxidation by Ce(IV), Ag(II), or $S_2O_8^{2-}$ results in the formation of $Co^{2+}(aq)$, albeit in less-than-quantitative yields. The proposed mechanism involves the formation of a one-electron-oxidized ligand radical coordinated to the Co(III) center which can engage in ligand-to-metal intramolecular electron transfer to form $Co^{2+}(aq)$ and the free two-electron-oxidized ligand in competition with further interaction with the oxidant. The primary questions in the induced electron transfer mechanism are the nature of the coordinated ligand-radical species and the kinetics of the intramolecular electron transfer step.

In order to gain some insight into the problem, we have used the reaction of the strongly oxidizing ($E°_{Red} = 2.8$ V)[5] OH radical with $Co(NH_3)_5py^{3+}$ (py = pyridine) as a model for the formation of $Co^{2+}(aq)$ via induced electron transfer.[6] Hydroxyl radicals are conveniently generated in the radiolytic decomposition of water according to reaction 1 with a G value

$$H_2O \rightsquigarrow e_{aq}^-, OH, H \qquad (1)$$

(number of radicals formed per 100 eV of energy absorbed) of 2.8; $G(e_{aq}^-) = 2.8$ and $G(H) = 0.55$. The techniques of radiation chemistry permit radicals of known stoichiometry to be generated selectively at desired rates with variable steady-state concentrations; pulse radiolytic generation of the radicals allows the kinetics and spectra of transient intermediates to be determined in the microsecond time frame. By the judicious use of scavengers, the primary radicals can be efficiently transformed: e_{aq}^- is quantitatively converted to OH

0020-1669/79/1318-2479$01.00/0